JSAE 20199285
SAE 2019-YY-YYYY

Effect of pressure cycling on gas exchange in a transparent fuel injector

Paul M. Abers[1], Emre Cenker[1], Koji Yasutomi[1,2], Joonsik Hwang[1], Lyle M. Pickett[1]
[1] Sandia National Laboratories, 7011 East Ave, 94550 Livermore, CA
[2] Hino Motors Ltd., Hino-shi, Tokyo

ABSTRACT

Gas ingested into the sac of a fuel injector after the injector needle valve closes is known to have crucial impacts on initial spray formation and plume growth in a following injection cycle. Yet little research has been attempted to understand the fate sac gases during pressure expansion and compression typical of an engine. This study investigated cavitation and bubble processes in the sac including the effect of chamber pressure decrease and increase consistent with an engine cycle. A single axial-hole transparent nozzle based on the Engine Combustion Network (ECN) Spray D nozzle geometry was mounted in a vessel filled with nitrogen, and the nitrogen gas pressure was cycled after the end of injection. Interior nozzle phenomena were visualized by high-speed long-distance microscopy with a nanosecond pulsed LED back-illumination. Experimental results showed that the volume of gas in the sac after the needle closes depends upon the vessel gas pressure. Higher back pressure results in less cavitation and a smaller volume of non-condensable gas in the sac. But a pressure decrease mimicking the expansion stroke causes the gas within the sac to expand significantly, proportional to the pressure decrease, while also evacuating liquid in front of the bubble. The volume of the gas in the sac increases during the expansion cycle due both to isothermal expansion as well as desorption of inherent dissolved gas in the fuel. During the compression cycle, the volume of bubbles decreases and additional non-condensable ambient gas is ingested into the sac. As the liquid fuel is nearly incompressible, the volume of both liquid and gas essentially remains constant during compression.

INTRODUCTION

Improvement of spray and the air-fuel mixing process in direct-injection engines is a key factor to achieve high-efficiency, clean combustion [1-2]. A thorough understanding of the entire spray process from transient needle opening and even after end of injection is essential for accurate spray prediction. Many experimental works have been carried out to elucidate the effects of hydraulic characteristics on spray penetration and plume dispersion, however, understanding of internal nozzle flow remains limited. To resolve this issue, real-scale transparent nozzles have been designed and employed for in-nozzle flow imaging research (e.g. [3-5]). Acrylic or quartz material offers optical access but also has a similar refractive index to diesel fuel, revealing sources of gas generation from cavitation or from mixing of non-condensable gas into the injector. One recent study [6] showed that the initial gas volume in sac and nozzle orifice significantly affects the initial spray development process. During injection, a substantial amount of time may be required to purge the gas and resume pure liquid injection. The injection of a mixture of gas and liquid fuel resulted in a larger plume width than the case which had a fully liquid filled condition [6].

Previous research has attempted to understand the interaction between cavitation and macroscopic spray characteristics under different nozzle geometries and injection conditions [7-9]. It is known that sharp edges around a nozzle orifice's inlet induces local pressure drops below the vapor pressure of fuel, resulting in cavitation bubbles [10]. For high-pressure fuel injectors, the cavitation bubbles generally survive until they reach the nozzle orifice outlet, affecting the atomization process and mixture profile of the delivered fuel. Cavitation sources include film-type cavitation along nozzle-inlet walls, and string-type cavitation where low-pressure, vortical structures form in the bulk liquid [11-14]. While cavitation tends to increase spray dispersion, string-type cavitation has been connected to the largest increases in spray spreading angle [14-16]. String-type cavitation is known to be highly transient, responding to changes in needle-valve lift.

While much of the knowledge about flow cavitation comes from steady-state experiments and models, there are strong motivations to better understand the transient processes for injection systems, including the opening and closing stages of injection, but also the behavior between multiple injections or cycles. For instance, in a short period of multiple injections, the final state in sac and nozzle orifice after previous injection affects the following injection spray process significantly [17]. Thus, initial condition in sac and nozzle orifice must be identified for precise injection control.

This study aims to provide better understanding regarding gas exchange processes within the injector after the needle closes and there are subsequent changes in charge-gas pressure. A real-scale transparent nozzle has been designed based on Engine Combustion Network (ECN) Spray D geometry for high-speed microscopic imaging. The spray tests were performed under emulated engine compression and expansion cycles with a programmable solenoid valve system. The first part of the discussion section describes the effects of ambient pressure on residual gas found within the sac and hole after needle closing. The second part presents how this gas changes depending on the simulated engine cycle.

EXPERIMENTAL SETUP

TRANSPARENT NOZZLE

An acrylic transparent nozzle was designed based on the ECN Spray D nozzle which has an outlet diameter of approximately 190 µm [18]. The acrylic material has a similar refractive index as the test fuel n-dodecane to provide clear visualization of internal flow with sensitivity to cavitation or ingested nitrogen gas when using backlit visualization. Additionally, acrylic has favorable mechanical properties for manufacture and clamping/sealing, while also enduring injection pressures to 100 MPa. Customized micro-machining tools were utilized to fabricate the sac and hole. Hydro-erosion was also applied to make a rounded hole inlet to match geometry and flow number of the metal ECN Spray D nozzle.

The shape of the transparent nozzle compared to the metal nozzle shape is shown in Fig. 1. The acrylic nozzle was submerged in a refractive index matching fluid to enable measurement of wall shape without optical distortion. The left image shows overlapping images of the metal nozzle (measured by x-ray tomography) slightly offset, and the transparent nozzle, indicating that the transparent nozzle matches the shape of the sac, hole inlet, and hole. The black spots are from deposits in the nozzle. Scanning electron microscopy (SEM) images of cut, gold-coated nozzle on the right side of Fig. 1 revealed that the transparent nozzle had surface textures on the order of 1 µm.

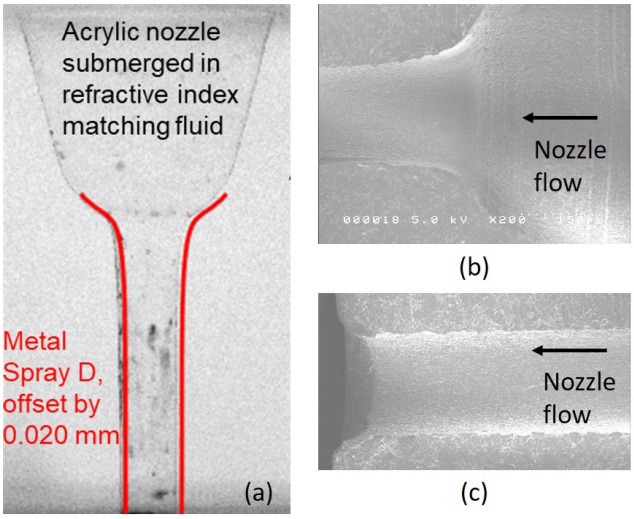

Fig. 1. (a) Overlapping images of acrylic nozzle and metal spray D outline (red), (b) SEM images of sac and nozzle orifice entrance, and (c) nozzle orifice exit.

The transparent nozzle was mounted at the tip of a modified ECN Spray C/D injector body. After removal of the needle, the original metal nozzle tip was ground and polished flat below the sealing surface. Reassembled, the original metal-metal needle valve surface is maintained. A schematic of the transparent nozzle and the injector assembly is shown in Fig. 2.

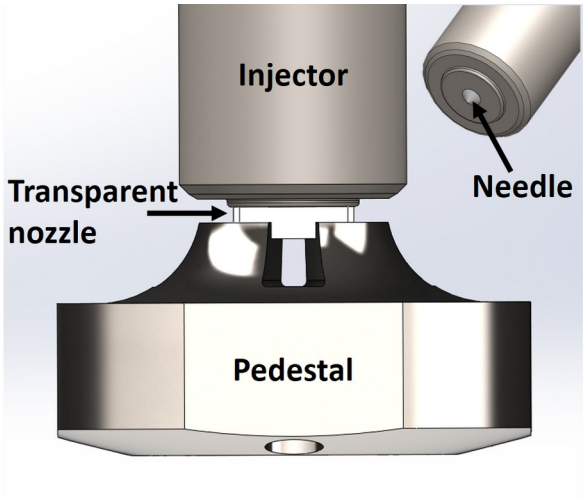

Fig. 2. A schematic of injector and transparent nozzle assembly.

The transparent nozzle was supported by a slotted pedestal on the bottom, providing optical access to both the internal flow and the emerging spray. A certain level of force was applied on the transparent nozzle by an injector installation clamp to form a seal between the ductile acrylic and the metal flat of the injector body. Locating tabs on the parts and translation screws on the pedestal provide nozzle/injector alignment.

SPRAY VESSEL

Experiments were carried out in an optically-accessible spray vessel as shown in Fig. 3. The vessel has four 25-mm diameter windows for line-of-sight optical access to the transparent nozzle. The chamber was designed small enough to allow short focal working distances. The space below the pedestal enables air entrainment into the spray but prevents back-splash of spray droplets. Nitrogen gas was delivered by an intake line adapter installed in one of the window. The air-fuel mixture after the injection was purged through an exhaust pipe at the bottom of the vessel.

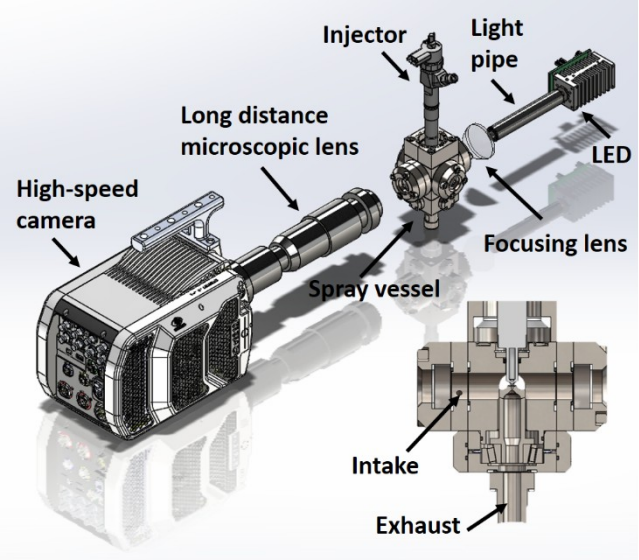

Fig. 3. A schematic of microscopic spray imaging system.

As a fuel, n-dodecane was used with a high-pressure syringe pump. The fuel was not degasified prior to injection experiments, so it contained a certain amount of dissolved gas as typical for a fuel exposed to air in a tank. For the experiments in this study, the fuel injection pressure was 500 bar and the ambient pressure was varied from 1 bar to 20 bar. The vessel temperature was not controlled and kept at room temperature. The vessel was equipped with a programmable solenoid valve system so the spray test could emulate engine compression and expansion, but not at the same time scale. For example, the compression cycle was mimicked by opening the intake solenoid valve and closing the exhaust solenoid valve. Similarly, the expansion cycle was performed by closing the intake solenoid valve and opening the exhaust solenoid valve.

High-speed imaging was conducted to capture cavitation and bubble processes after the injection. A high-speed camera (Phantom v2512) with a long-working-distance microscopic lens (Infinity K2) was used. The sampling rate was set to 80,000 frames per second (fps) to understand processes on the time scales of injection, and 500 fps for slower pressure cycling tests after the end of injection. The image resolution was 4.65 µm per pixel. Back illumination was provided by a blue LED with a wavelength of 455±11 nm. The LED operating pulse was synchronized to high-speed camera shutter signals. The pulse duration for the LED was set to 100 ns to freeze the two-phase flow independent of the camera exposure time.

IMAGE PROCESSING

An in-house MATLAB code was used to measure the amount of gas in the nozzle. The images were normalized by a set of averaged values from the images prior to the injection. Due to the matching refractive index of the fuel and back lighting, liquid or nozzle regions appear bright while bubbles of cavitation or gas appear dark because of scattering/extinction gas/liquid interfaces. Images of large bubbles were inverted, binarized with a threshold value, and then fit to circular Hough Transform to determine their diameter.

Fig. 4 shows the images before and after the image processing. The bubbles found by the code were presented by red dashed lines.

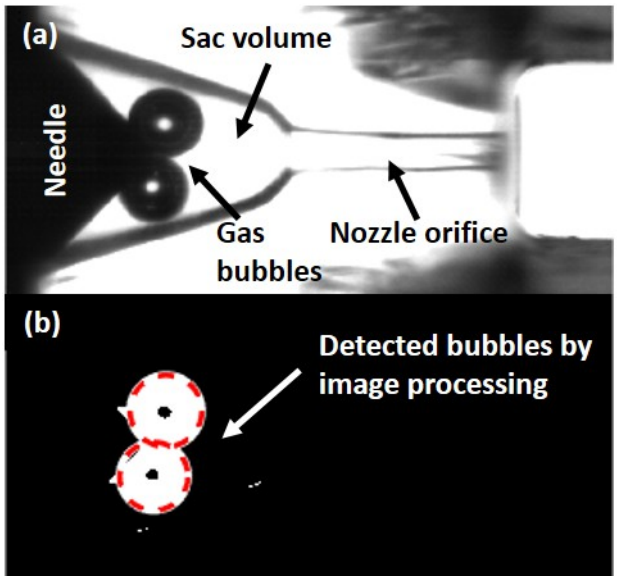

Fig. 4. (a) raw image in sac and nozzle orifice after needle close (b) bubble detection by image processing (red dotted means bubbles, online movies available at [19]).

The Hough Transform function returns the center and radius of the circles it finds, and these radii were then used to calculate the area and volume of the gas bubbles in the sac. The performance of the circle recognition routine was verified by comparing the transformed volume and the total number of bright pixels (total projected area) in the region of interest. Although the total pixel counting is a simpler method, it is inherently a two-dimensional information and the exact volume cannot be extracted in the case of an image with multiple bubbles.

Fig. 5 shows a plot of pressure, binarized (projected) area based on bright pixel counting, transform area and transform volume versus time after end of injection (aEOI) along with the snapshots of the raw images at five instants. This data was taken for an

expansion cycle starting at a back pressure of 10 bar in the chamber and falling to 1 bar. The time stamps are shown at the top of each raw image and corresponding information on the scatter plot is indicated with arrows. The area and volume measurements obtained by Hough Transform are in good agreement with the binarized area. The trend of the bubble sizes can also be seen on the raw images. This comparison shows that the binarized area can be also used as an indicator to describe the bubble volume change trends. Later in this study, some comparisons are performed by means of binarized area.

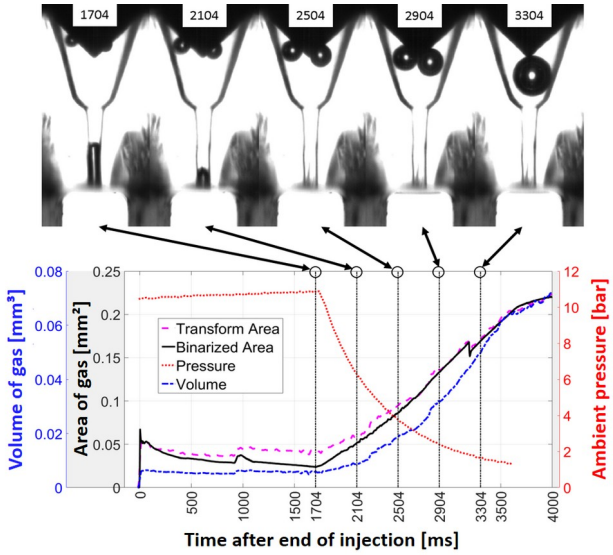

Fig. 5. Assessment of image processing and bubble volume measurements based on 10 bar to 1 bar expansion cycling result.

One of the limitations of this study is that the image processing was performed with a camera pointing in one direction only, resulting in a two-dimensional look into the nozzle and chamber. When trying to determine bubble volume, some bubbles may be missed due to stacking along the line-of-sight or from being blocked by the injector tip. The overlap along a line-of-sight overlap could be confirmed by the other orthogonal camera in some instances, but was not automated in post-processing. Therefore, the gas volume calculated/measured would be expected to be less than the actual volume. Sharp changes in calculated volume appear if bubbles block along a line of sight or if bubbles coalesce.

Another limitation in processing is when the Hough Transform is performed when bubbles are too dense. If too many bubbles are present or there is incomplete stacking (two bubbles that have a partial stacking and their resulting shape appears oblong), then the routine could not recognize any (or some) of the bubbles. This can lead to random plummets in the volume for specific times in the graph. To combat this, if a value for the volume was less than one fifth that of the previous several values, the previous volume was used for that value. Also, a moving median and Gaussian filter was used on the data to reduce the noise and random failures in the Hough Transform. In the end, the limitations of the imaging and code did not affect conclusions of the research.

RESULTS AND DISCUSSION

EFFECTS OF AMBIENT PRESSURE ON CAVITATION PROCESS

The effect of ambient pressure (nitrogen back pressure) on cavitation and gas exchange is presented in Fig. 6. Images are shown for time sequences corresponding to the end of injection at ambient pressures of 1 bar and 20 bar. The time stamps show time after end of needle close, which we note is different/earlier than the time when liquid stops leaving the hole (being injected). For each image, internal flow is visible at the left and spray injection development is visible at the right. Because the lens was focused on the sac and orifice region, the emerging spray looks blurry and out of focus. The area with higher light intensity means pure liquid phase of the fuel, whereas dark regions are from gas/liquid mixtures.

The first image for steady (high needle lift) timings does not show evidence of internal cavitation within the needle seat, sac, or hole. Bubbles (gas-phase) appear as the needle closes. Understanding the type of gas, whether fuel vapor from cavitation or from non-condensable gas (nitrogen) mixed into the sac or released from dissolved liquid, requires analysis of the time history. The first instances of bubbles at sudden closure of the needle are from cavitation sources [6]. Pressure inside the sac drops below the fuel vapor pressure in local regions, allowing transition to vapor and also releasing any dissolved gas in the liquid. These first cavitation zones appear at the needle seat region, but also in the bulk of the sac. High-speed movies [6] convincingly show cavitation in the bulk of the sac may or may not flow/ originate from the needle-seat region. Previous large-eddy simulations (LES) of Battistoni et al. [20] performed under similar test conditions to this study showed cavitation only in the needle seat region, but the experimental data shows cavitation also in the bulk region downstream of the needle. The bulk cavitation creates extra volume which displaces liquid out of the injector as a form of liquid ligaments or dribble.

The cavitation in the bulk of the sac is momentary. As pressure equilibrates in the sac, the cavitation vapor pocket collapses. As this volume of fuel vapor decreases, non-condensable nitrogen gas is entrained (ingested) from the orifice exit into the sac to replace this volume. These gas bubbles remain for very long periods after the end of injection, when pressure is constant, confirming that they are not fuel vapor in a cavitating state, but rather nitrogen mixed with only a low fraction of fuel vapor (i.e, fuel vapor at low concentration—partial pressures at the fuel vapor pressure). Our observation on gas exchange process, facilitated by high-speed imaging, matches

a hypothesis of Swantek and coworkers [21] that the remaining gas bubbles in the sac and orifice after the injection was derived by gas ingestion rather than fuel vapor generation due to lower pressure. This gas exchange process is observable at all ambient pressures in this study.

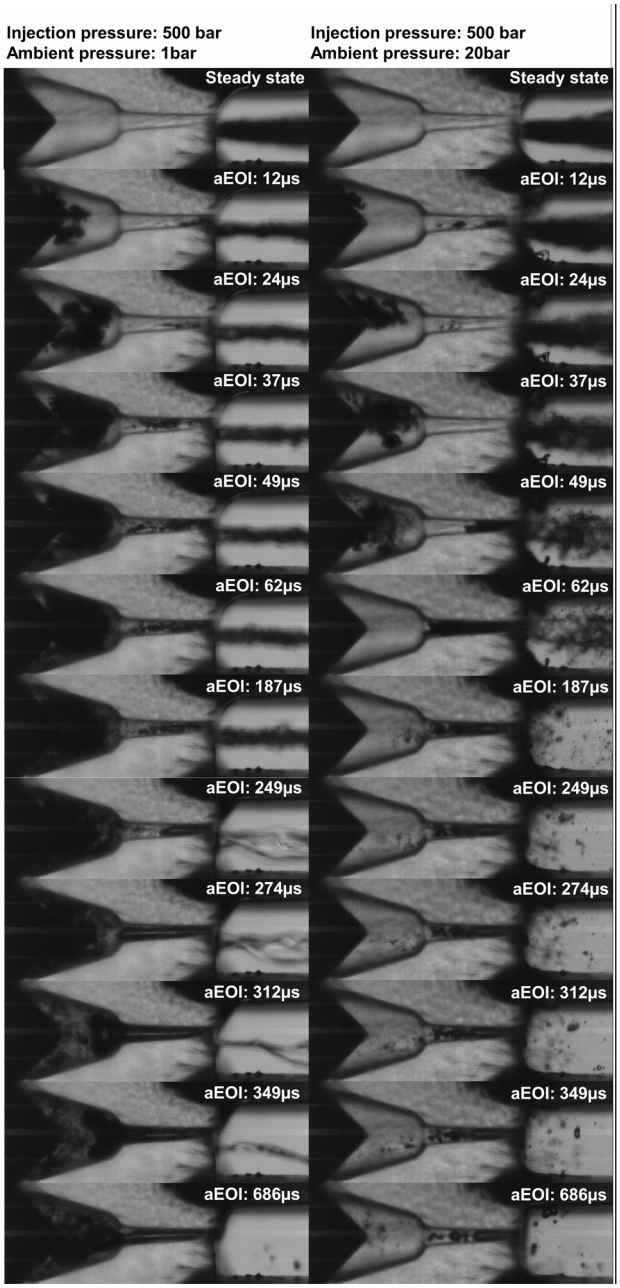

Fig. 6. Bulk cavitation and gas ingestion process under ambient pressure of 1 bar (left) and 20 bar (right) conditions.

A comparison of the 1 bar and 20 bar conditions long after the end of injection clearly shows that there is more gas at 1 bar, to the level that much of the sac remains obscured by gas. An initial assessment for the amount of gas is found by calculating the projected area of gas bubbles as a function of time, as shown in Fig. 7 for other ambient pressures. Each curve is an ensemble average of five measurements. The error bars indicate the standard deviation calculated from this averaging.

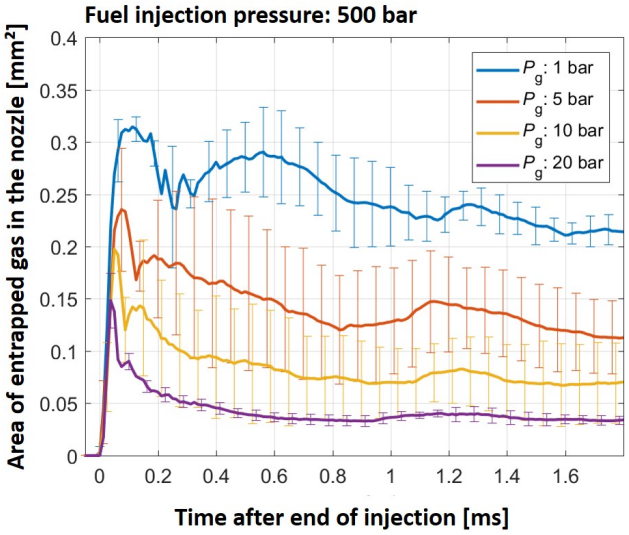

Fig. 7. Projected gas bubble area in the sac and nozzle orifice at an injection pressure of 50 MPa.

The figure confirms that the total gas volume in the sac and orifice after the injection decreases with increasing ambient pressure. The first peaks in the graph show gas bubble formation due to the rapid vaporization of liquid fuel (bulk cavitation). As expected, a higher ambient pressure also raises any minimum pressure within the sac, creating less bulk cavitation at higher ambient pressures. The duration of fuel vapor cloud existence is also shorter under higher ambient pressure. After the fuel vapor cloud disappears (collapse of the cavitation), the projected gas area fluctuates with pressure oscillation as well as randomly rotating bubbles in the sac and orifice area. The projected area of gas bubbles at 1 bar was approximately 5.5 times larger than that at 20 bar. This result shows a rough correlation of residual gas content in the sac and orifice dependent upon ambient pressure. However, note that there are many overlapping gas bubble regions at 1 bar, making quantification of gas bubble volume difficult for this condition.

While the data provided in Fig. 7 show what looks like a stabilizing trend during the first milliseconds after injection, data taken on a longer time scale shows that the perceived gas volume has not stabilized and is not at equilibrium. Figure 8 shows internal-nozzle imaging with 10 bar ambient gas pressure maintained for over 1 s after the end of injection. The image immediately after the end of injection shows many bubbles. A high-speed movie for this event (available online at [21]) shows that bubbles convect and coalesce, many flowing towards the needle. However, the bubbles marked as A and B do not coalesce with other bubbles. A careful tracking of these bubbles reveals that their diameters decrease in time. By 1 s after the end of injection, Bubble A is no longer visible, and the movie shows that it has not passed behind the needle. While many bubbles do pass behind the needle, or in contact with the needle, there are many other smaller bubbles that do not coalesce with other bubbles and that also disappear to view, just like Bubble A. Also, the larger

bubble that comes in contact with the needle seat on the top right clearly is decreasing in diameter.

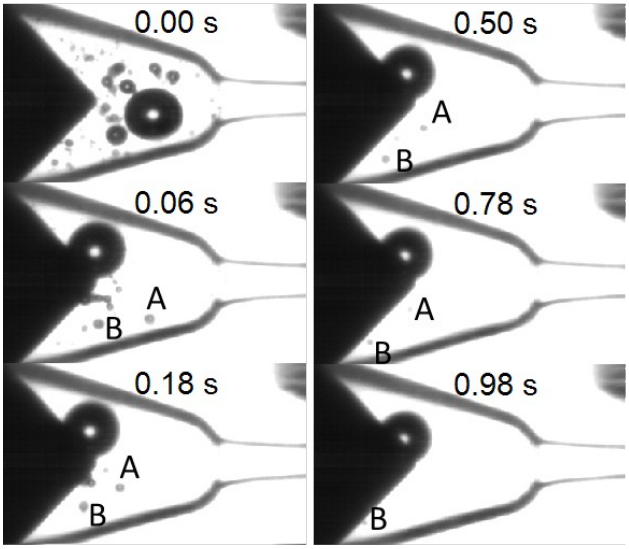

Fig. 8. Visualization in the sac and hole long after the end of injection with injection pressure of 500 bar and ambient gas pressure of 10 bar. Imaging/lighting was saturated to highlight bubble dynamics. Time after end of injection is given at top of image (online movies available at [19]).

The decrease in gas volume and disappearance of smaller bubbles are indicators that nitrogen gas dissolves into the liquid fuel when held at pressure after the end of injection. The rapid mixing between gas and liquid initiated at the end of injection creates a system that is not at equilibrium. Liquid (which had little dissolved gas) comes into contact with a much larger amount of gas within the sac. Given more time, the nitrogen gas dissolves into the liquid.

While Fig. 8 shows that the gas volume varies with time, even when the gas pressure is constant after the end of injection, and there are additional complexities caused by the dynamics for bubbles moving into contact with solid surfaces, the imaging sequence reveals that some gas is stored/dissolved in the liquid after the end of injection. Understanding that gas can be dissolved into the liquid, at mass concentrations greater than the original liquid fuel, is helpful when considering the effect of expansion or compression cycling of the ambient pressure.

EFFECTS OF PRESSURE CYCLING ON BUBBLE DYNAMICS

The ambient pressure after the injection was controlled by a programmable solenoid valve system to investigate bubble dynamics under emulated engine cycles. An expansion cycle was emulated by opening the exhaust valve in the vessel, typically after the end of injection. Typical expansion cycles with different initial gas pressure are depicted in Fig. 8, which shows pressure decline in less than 2 s. While this is a much longer time than a working engine, the change in pressure provides an opportunity to observe the physics of gas/liquid exchange during these pressure cycles.

The gas volume in the sac and orifice region was computed during pressure cycling. Note that bubbles move rapidly in the sac and tend to coalesce after the end of injection. As demonstrated in Fig. 8, bubbles may also dissolve into the liquid. In general, the coalescence or drift of bubbles yields bubbles that are separated and that can be tracked for volumetric analysis more clearly, and this typically occurs within 10-20 ms after the end of injection. If pressure is maintained constant for a longer time, like Fig. 8 (with 1 s), there is more absorption of gas but the remaining bubbles are also more exposed for analysis. Please refer to the online movies [21] for examples. Therefore, these bubbles may be studied clearly as pressure decreases after the end of injection.

Bubbles that could clearly be tracked in the hole and sac were then treated using the Hough transform method. Analysis may be stopped if the bubble makes it to the edge of nozzle or sac, making the volume analysis more complex. The volume is given in Fig. 9, which corresponds to the same pressure decay given in Fig. 10. The final gas volume after expansion maintains the same rank ordering as the initial gas volume, even though the high-pressure conditions had the potential for more gas expansion. A simple explanation is that the initial gas content more than offsets the effect of gas expansion, or expressing it differently, that the mass of gas initially in the sac is actually smaller at high pressure. We will expand upon this point in more detail below.

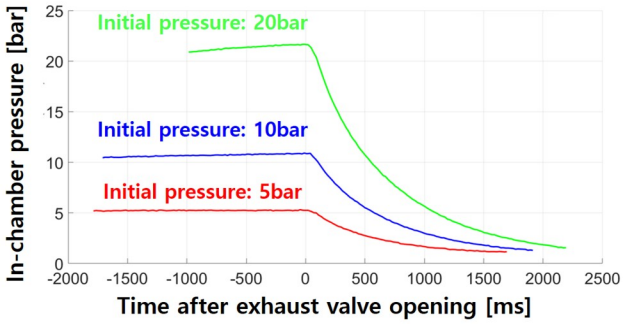

Fig. 9. In-chamber pressure during expansion cycle spray test (exhaust valve opened at 0 ms).

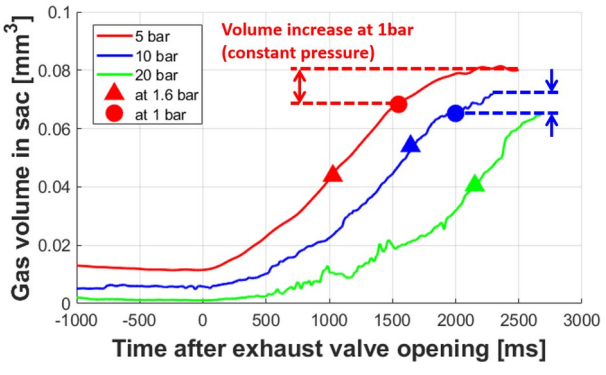

Fig. 10. Volume of gas volume in sac in expansion cycle under different ambient pressure conditions.

The rate of expansion for the three cases is also different right after the expansion begins. In the 5 bar case, expansion begins to take place immediately showing a larger slope in gas volume increase rate after exhaust valve open. The 10 bar case showed a slower gas expansion with a certain delay, but eventually it too follows a similar rate to that of the 5 bar case. The 20 bar case expands slowly at the beginning, but it also reaches a similar rate of increase as that of the other cases, with a longer delay reaching that point. The point at which the expansion of the bubbles starts to increase rapidly appeared to correlate with the pressure in the vessel. The expansion increases rapidly once the pressure falls below about 7 bar. The bubble expansion continued even after the ambient pressure reached 1 bar. The result beyond circle symbol presents the gradual volume increased under constant pressure. This means the desorption of dissolved gas in the fuel was still occurring.

While some differences are expected because the pressure change with time is different for each condition, a pressure-volume plot removes the time element differences as given in Fig.11. In this format, the relationship between volume and pressure shows a more universal trend, but the final volume at 1 bar remains different. Ultimately, identification of the thermodynamic gas expansion path would be helpful because, with knowledge of the gas in the sac immediately after injection, one could reliably predict the volume of gas within the injector after expansion. This volume could then be used for CFD simulations for the next injection, with better understanding for the initial sac conditions. For this study, limits for the expansion process were analyzed by assuming either isothermal or isentropic expansion when compared to experimental data.

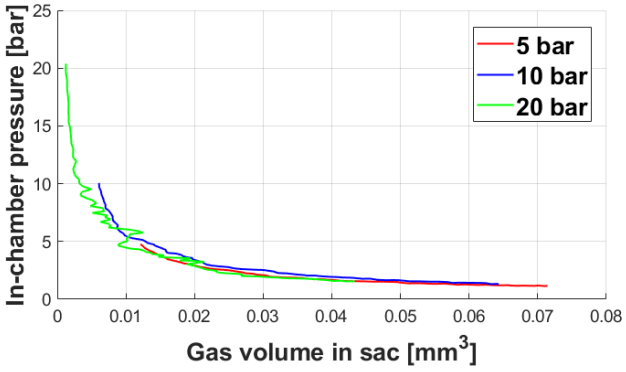

Fig. 11. Relationship between in-chamber pressure and gas bubble volume under different expansion cycling conditions, (online movies available at [19]).

Beginning with the initial pressure P_1 and volume V_1, Equation 1 shows the relationship for predicted volume V_2 in a closed system where γ is 1.0 for an isothermal process or 1.4 for an isentropic process with nitrogen near 300 K.

$$P_1 V_1^{\gamma} = P_2 V_2^{\gamma} \qquad \text{eq (1)}$$

Figures 12, 13, and 14 show the measured *P-V* curve compared to the theoretical expansion paths for each initial chamber pressure. The blue lines are thermodynamic expansion from the initial volume, meanwhile, the black curves are derived as compression from the final volume of the experimental result.

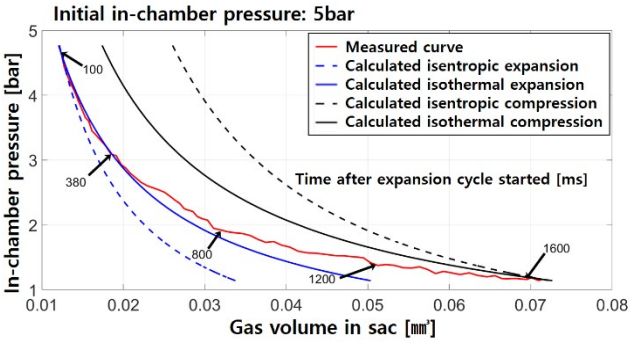

Fig. 12. Comparison between theoretical isothermal (solid blue, black) / isentropic (dotted blue, black) process and experimental result (red) under 5 bar to 1 bar expansion cycle (Blue lines show expansion process from the initial point, while black lines present compression from the end point).

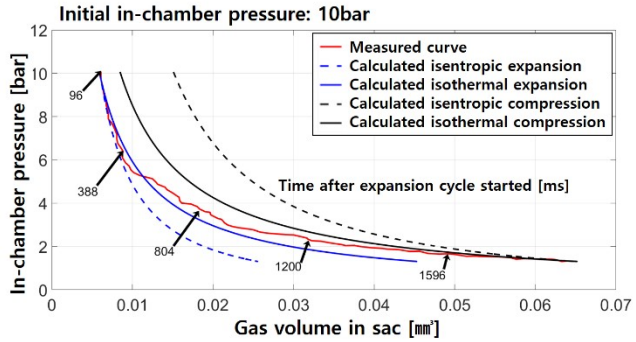

Fig. 13. Comparison between theoretical isothermal (solid blue, black) / isentropic (dotted blue, black) process and experimental result (red) under 10 bar to 1 bar expansion cycle.

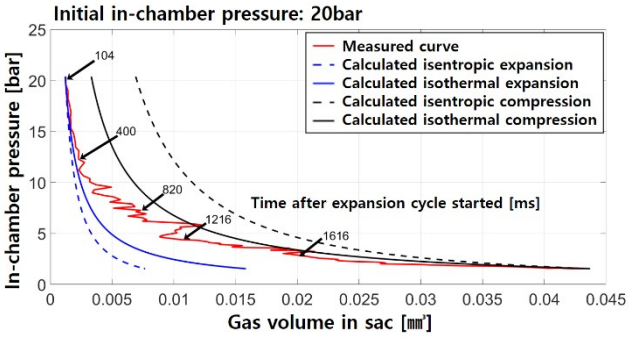

Fig. 14. Comparison between theoretical isothermal (solid blue, black) / isentropic (dotted blue, black) process and experimental result (red) under 20 bar to 1 bar expansion cycle.

Considering all of the ambient pressures, the general observation is that there is more volumetric expansion than either isentropic or isotropic expansion. The expansion curve begins much closer to isothermal expansion, rather than isentropic expansion. For example, there is a close tracking of isothermal expansion curve up until 400 ms after start of expansion for the 5 bar condition (Fig. 11). Expansion that is more isothermal than isentropic (adiabatic) may be expected because each bubble is surrounded by liquid fluid with large heat capacity and high surface area. Consequently, temperature change (decrease and small volume expansion) is apparently less likely.

Ultimately, as pressure decreases the volumetric expansion becomes greater than isothermal expansion, which indicates that additional sources of gas must be considered. One explanation is bubbles that may have been hidden from analysis coming into view. While this could occur in isolated events, there is ample evidence that volume increases faster than isothermal expansion when these events are not occurring. After reviewing the high-speed image series for the Hough Transform for each case, there does not appear to be any bubble that becomes recognized that was not previously recognized that would affect the curve for any of the three cases. Furthermore, if a bubble did become recognized that was not previously recognized, then the measurement curve should have a noticeable jump from its current value to a much greater value. In the 20 bar case there is a large jump in the measurement curve in between times 820ms and 1,216 ms. This is an example of a bubble being recognized that was not previously recognized.

Since the increase above theoretical values for the expansion curve cannot be attributed to a new bubble appearing, the only remaining explanation for the additional volume is desorption of dissolved gas from the fuel. The sequence shown in Fig. 8 conclusively shows that gas dissolves into the liquid prior to expansion. As pressure decreases, this gas will come out of the liquid solution, particularly at nucleation sites where there are already bubbles or surface pores, and add to the total gas volume.

Additional evidence for the desorption of dissolved gas is the finding that bubble gas volume continues to increase, even after pressure reaches 1 bar and stops decreasing. Figure 10 indicates the instant when pressure decreases to 1 bar and is constant thereafter. The rate of gas volume increase slows, but does not stop at this time. Volume continues to increase by approximately 10% for both the 5 bar and 10 bar cases, before analysis has to stop because gas begins to move into the hole. Indeed, gas volume continues to increase afterwards but is difficult to quantify. Therefore, volumetric expansion continues even when pressure is not changing, which causes further departure from the closed-system, isothermal expansion. The volume addition from desorbed gas, which signifies an open system rather than a closed system, also explains why the compression cycle of the final volume (black lines in the figures) does not follow an isentropic or isothermal compression that would match the data.

Assuming the isothermal expansion process as the ideal cycle, we estimate the volume of desorbed gas for each case at the time of complete expansion (to 1 bar) as given in Table 1. The table includes volume data at three different ambient pressure (1.6 bar, 1bar and 3ms after in-chamber pressure reached 1 bar) during expansion process. Table 1 shows when in-chamber pressure was 1.6 bar, the volumetric increase for 5 bar, 10 bar and 20 bar initial pressure cases was 13.7%, 29.4%, and 59.8%, respectively. This finding is in agreement with Henry's law equilibrium analysis, supporting the idea that more gas is dissolved into the liquid initially at high pressure, and therefore proportionally more gas will come out of solution when the pressure decreases. As discussed in Fig 10, a lot of desorption was occurred during the constant ambient pressure at 1 bar.

Table 1. Calculated volume change during expansion cycle.

		Measured at in-chamber pressure [bar]		
Initial P. Volume[10^3mm^3]	Volume [10^3mm^3]	1.6	1	3ms after 1bar
5 bar ($V_{initial}$=12.1)	V_{nozzle}	43.8	68.3	76.3
	$V_{desorp.}$	6	7.8	15.8
10 bar ($V_{initial}$=6.1)	V_{nozzle}	54	65.2	71.5
	$V_{desorp.}$	15.9	4.2	10.5
20 bar ($V_{initial}$=1.3)	V_{nozzle}	40.5		
	$V_{desorp.}$	24.2		

Having discussed the effect of ambient pressure on the gas in the sac at the end of injection, and its expansion and desorption during an expansion cycle, we now address the effect of compression on gas within the sac. A compression cycle was investigated by pressurizing the chamber with solenoid valves, in reverse of the expansion cycle simulation. Fig. 15 shows a chronological progression of images during a time of interest right as compression begins. The sequence begins after an expansion cycle and a static initial pressure of 1 bar for approximately 3 s, as shown in the pressure traces given in Fig. 16.

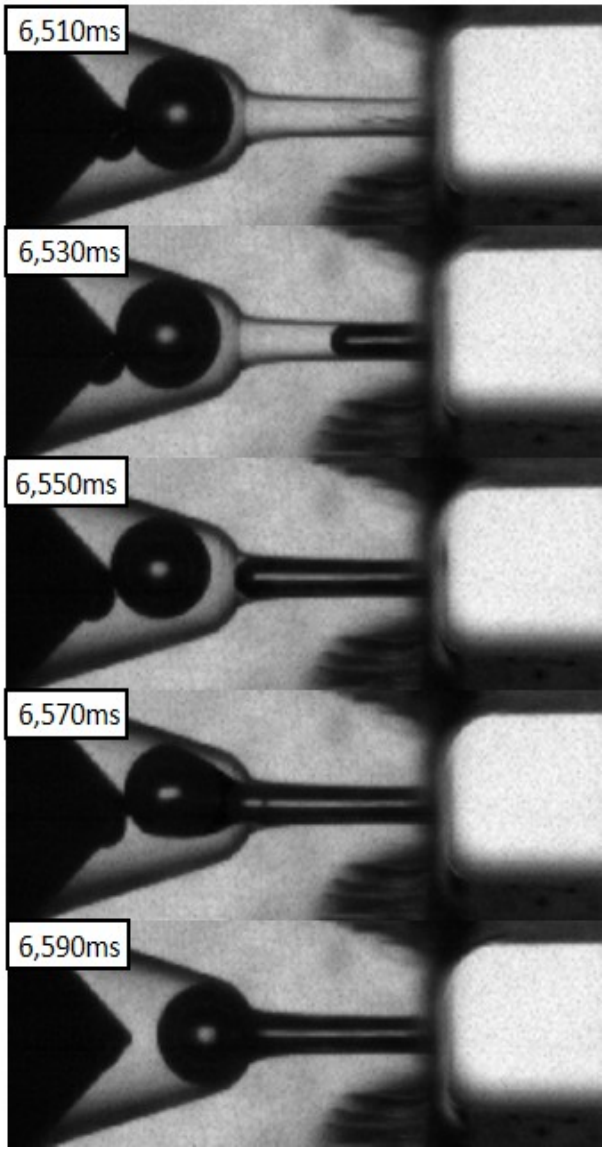

Fig. 15. Images of gas bubble during compression cycle (time stamp on the left top corner presents time after end of injection and the in-chamber pressure at each frame corresponds to the values in Fig. 16., online movies available at [19]).

At the beginning of compression, there are two different bubbles. One large bubble is at the hole inlet and another smaller bubble is near the needle tip. As pressure increases in the chamber, gas flows into the hole and liquid displaces the bubble towards the needle tip. The volume of the two bubbles now decreases because of compression, but at one point (with chamber pressure less than 2 bar) the two bubbles coalesce and also merge with the gas from the hole, with the internal bubble moving back towards the hole inlet. After this rearrangement of the gas volume, with the hole filled with gas and the bubble at the hole inlet, the liquid and gas remain in this position (the bottom image in Fig. 15) throughout compression from 2 bar to 12 bar. There is no discernable increase or decrease in the gas volume despite the massive change in pressure.

The overall explanation for this behavior (during compression) is that the overall volume of liquid within the sac and hole remains unchanged during compression. The bubbles inside the nozzle compress with the increasing pressure and the forcing of liquid from the hole into the sac region. But as an incompressible fluid (for modest changes in pressure from 1 to 12 bar), the liquid fuel volume is not expected to change. This explains why the liquid and gas positions do not change after the initial rearrangement. Note that significant mass of pressurized nitrogen enters the hole and into the sac during pressurization. Some nitrogen gas may also dissolve into the liquid, but the liquid volume does not change.

To acquire a quantitative result, the volume of the bubble was calculated by image processing. Fig. 16 shows the volume versus time during the whole pressure cycle.

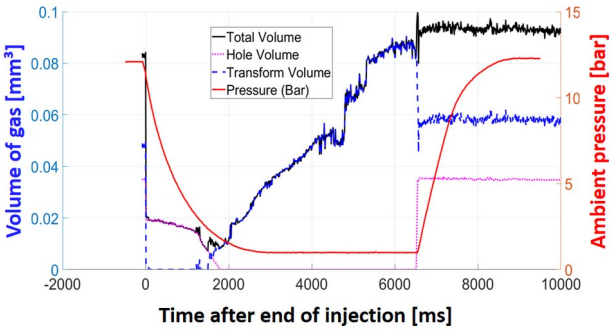

Fig. 16. Volume change in sac and nozzle orifice during combined expansion and compression cycle.

In the graph, the transform volume refers to the volume in the sac calculated via the Hough Transform for finding circles. The hole volume refers to the volume in the hole of the nozzle. The hole volume was calculated by taking the binarized area calculated in the hole of the nozzle and dividing by the width of the hole (which was found by determining the pixel width in the image and then multiplying by the scale of the images). This resulted in the length into the hole that the volume had filled. Then, the hole is assumed to be a cylinder and its volume is calculated using the length into the hole as the height of the cylinder, and the width of the hole (used earlier to calculate the length into the hole) as the diameter of the circular face of the cylinder. The total volume is simply a sum of the transform and hole volumes. The calculation confirms that the compression cycle does not decrease the volume in the nozzle (sac and hole). Here, we see an instance of the Hough Transform failing. The Hough Transform fails to recognize the whole volume of the amorphous shape at time 6,570 ms and instead only recognizes a portion of it, which results in the sharp drop on the graph for the total and transform volumes. Then in the next frame, the Hough Transform once again recognizes the volume of the bubble as it has returned to a circular shape. The graph illuminates the fact that during the compression cycle, the total volume of gas inside the

sac does not change, rather the volume is just rearranged.

While the compression cycle results in the expected result that the liquid volume does not change, the manner in which the gas aligns relative to the liquid is critical information to understand the initial gas and liquid conditions at the beginning of injection after compression. In addition, the forcing of hot gases into the sac by compression could vaporize some liquid fuel in an engine. Also, the significant mass of gas entering inside passages of the injector is a mechanism for the mixing of cylinder contents (soot, residuals, deposits) that could ultimately foul the injector.

CONCLUSION

A high-speed microscopic backlit imaging study was performed to study cavitation and bubble dynamics in sac and nozzle orifice. A single-hole transparent nozzle based on ECN Spray D geometry was designed with acrylic material. Detailed gas exchange processes were revealed by image processing techniques.

The experimental results showed that the ambient pressure in the spray vessel played a key role in the leftover quantity of gas volume in the sac and nozzle orifice. After the needle close, the amount of bulk cavitation and gas ingestion into the sac volume was decided by the ambient pressure. Higher ambient pressure attributed much less bulk cavitation and gas ingestion compared to lower ambient pressure conditions. The ingested gas dissolves into the liquid when held at constant pressure. During a pressure decrease simulating cycle expansion, gas bubbles tended to expand closer to the theoretical isothermal expansion instead of along isentropic expansion. But the gas volume also increases significantly because of desorption of the initially dissolved gas. Meanwhile, in the compression cycle, the total volume of liquid fuel in the sac and hole did not change, following expectation for the liquid as an incompressible liquid. The volumes of gas initially within the injector rearrange to position gas within the hole and inlet to the hole, which is a more likely position for gas at the beginning of the next injection after compression.

ACKNOWLEDGMENTS

The funding for the project was provided by the Spray Combustion Consortium of automotive industry sponsors, including Convergent Science Inc., Cummins Inc., Ford Motor Co., Hino Motors Ltd., Isuzu Motors Ltd., Groupe Renault, and Toyota Motor Co., with experimental facilities supported by the U.S. DOE Office of Vehicle Technologies.

The high-speed microscopy experimental study was performed at the Combustion Research Facility, Sandia National Laboratories is a multi-mission laboratory managed and operated by National Technology and Engineering Solutions for Sandia LLC, a wholly owned subsidiary of Honeywell International, Inc., for the U.S. Department of Energy's National Nuclear Security Administration under contract DE-NA0003525.

REFERENCES

1. Dec, John E. *A conceptual model of DI diesel combustion based on laser-sheet imaging*. No. 970873. SAE technical paper, 1997.
2. Dec, John E. "Advanced compression-ignition engines—understanding the in-cylinder processes." *Proceedings of the combustion institute* 32, no. 2 (2009): 2727-2742.
3. Arcoumanis, C., Flora, H., Gavaises, M., Cavitation in real-size multi-hole diesel injector nozzles. No. 2000-01-1249. SAE Technical Paper, 2000.
4. Blessing, M., König, G., Krüger, C., Michels, U., & Schwarz, V. (2003). Analysis of flow and cavitation phenomena in diesel injection nozzles and its effects on spray and mixture formation. *SAE transactions*, 1694-1706.
5. Li, H., & Collicott, S. H. (2006). Visualization of cavitation in high-pressure diesel fuel injector orifices. *Atomization and sprays*, *16*(8).
6. Manin, J., Pickett, L., Yasutomi, K., Transient cavitation in transparent diesel injectors, 14th ICLASS 2018.
7. Roth, H., Gavaises, M., & Arcoumanis, C. (2002). *Cavitation initiation, its development and link with flow turbulence in diesel injector nozzles* (No. 2002-01-0214). SAE Technical Paper.
8. Han, J. S., Lu, P. H., Xie, X. B., Lai, M. C., & Henein, N. A. (2002). *Investigation of diesel spray primary break-up and development for different nozzle geometries* (No. 2002-01-2775). SAE Technical Paper.
9. Tamaki, N., Shimizu, M., Nishida, K., & Hiroyasu, H. (1998). Effects of cavitation and internal flow on atomization of a liquid jet. *Atomization and Sprays*, *8*(2).
10. Liu, Z., Im, K. S., Wang, Y., Fezzaa, K., Xie, X. B., Lai, M. C., & Wang, J. (2010). *Near-nozzle structure of diesel sprays affected by internal geometry of injector nozzle: visualized by single-shot X-ray imaging* (No. 2010-01-0877). SAE Technical Paper.
11. Gavaises, M., Andriotis, A., Papoulias, D., Mitroglou, N., & Theodorakakos, A. (2009). Characterization of string cavitation in large-scale Diesel nozzles with tapered holes. *Physics of fluids*, *21*(5), 052107.
12. Andriotis, A., Gavaises, M., & Arcoumanis, C. (2008). Vortex flow and cavitation in diesel injector nozzles. *Journal of Fluid Mechanics*, *610*, 195-215.
13. Reid, B. A., Hargrave, G. K., Garner, C. P., & Wigley, G. (2010). An investigation of string cavitation in a true-scale fuel injector flow

geometry at high pressure. *Physics of Fluids*, *22*(3), 031703.
14. Gavaises, M. & Andriotis, A. (2006). *Cavitation inside multi-hole injectors for large diesel engines and its effect on the near-nozzle spray structure* (No. 2006-01-1114). SAE Technical Paper.
15. Hayashi, T., Suzuki, M., & Ikemoto, M. (2013). Effects of internal flow in a diesel nozzle on spray combustion. *International Journal of Engine Research*, *14*(6), 646-654.
16. Watanabe, H., Nishikori, M., Hayashi, T., Suzuki, M., Kakehashi, N., & Ikemoto, M. (2015). Visualization analysis of relationship between vortex flow and cavitation behavior in diesel nozzle. *International Journal of Engine Research*, *16*(1), 5-12.
17. Herfatmanesh, M. R., Peng, Z., Ihracska, A., Lin, Y., Lu, L., & Zhang, C. (2016). Characteristics of pressure wave in common rail fuel injection system of high-speed direct injection diesel engines. *Advances in Mechanical Engineering*, *8*(5), 1687814016648246.
18. Engine Combustion Network webpage: https://ecn.sandia.gov/
19. "Engine Combustion Network | Sac bubble expansion." [Online]. Available: https://ecn.sandia.gov/pub-links/jh001/sac-bubble-expansion
20. Battistoni, M., Xue, Q., & Som, S. (2016). Large-Eddy Simulation (LES) of spray transients: start and end of injection phenomena. *Oil & Gas Science and Technology–Revue d'IFP Energies nouvelles*, *71*(1), 4.
21. Swantek, A. B., Duke, D., Tilocco, F. Z., Sovis, N., Powell, C. F., & Kastengren, A. L. (2014). End of injection, mass expulsion behaviors in single hole diesel fuel injectors. *Proceedings of ILASS Americas, Portland OR*.

CONTACT

Corresponding author

*Lyle M. Pickett – LMPicke@sandia.gov

Combustion Research Facility (CRF), Sandia National Laboratories, 7011 East Ave, 94550 Livermore, CA, USA